Brain, Behavior and Evolution

Brain Behav Evol 2002;59:199–210

Modeling Electrosensory and Mechanosensory Images during the Predatory Behavior of Weakly Electric Fish

Mark E. Nelson[a] Malcolm A. MacIver[b] Sheryl Coombs[c]

[a]Beckman Institute for Advanced Science and Technology and Department of Molecular and Integrative Physiology, University of Illinois at Urbana-Champaign, Ill., [b]Division of Engineering and Applied Science, and Computation and Neural Systems Program, California Institute of Technology, Pasadena, Calif., [c]Parmly Hearing Institute and Biology Department, Loyola University Chicago, Chicago, Ill., USA

Key Words
Dipole · Electrolocation · Electroreception · Electrosensory · Lateral line · Mechanosensory · Prey capture · Weakly electric fish · Sensory ecology · Natural images

Abstract
Black ghost knifefish (*Apteronotus albifrons*) are nocturnal, weakly electric fish that feed on insect larvae and small crustaceans in the freshwater rivers of South America. In the absence of visual cues, prey detection and localization in this species is likely to rely on weak electrosensory and mechanosensory cues generated by the prey. In this paper, a modeling approach is used to estimate contributions to prey capture behavior from three octavolateralis modalities: the high- (tuberous) and low- (ampullary) frequency components of the electric sense and the high-frequency (canal neuromast) component of the lateral line mechanosensory system. For each of these modalities, the physical stimulus generated by the prey is approximated using a simple dipole model. Model parameters are constrained using previously published data as well as new empirical data on the electrical impedance characteristics of *Daphnia magna*. Models of electrosensory and mechanosensory stimuli are combined with actual prey strike trajectories from infrared video recordings to reconstruct spatial images of the prey along the sensory surface of the fish during the behavior. Modeling results suggest that all three modalities might contribute and that the relative contributions may change as a function of environmental conditions (e.g., water conductivity) and as a function of time over the course of the prey capture event.

Introduction

Black ghost knifefish (*Apteronotus albifrons*) are nocturnal, weakly electric fish that feed on insect larvae and small crustaceans in freshwater rivers of South America [Hagedorn, 1986; Winemiller and Adite, 1997]. When hunting in the dark, the fish can potentially utilize information from multiple non-visual modalities to detect physical stimuli arising from the prey. The mechanosensory lateral line system can be stimulated by small pressure gradients arising from swimming movements of the prey or from the differential movement between predator and prey. The low-frequency, or passive, electrosense (ampullary system), can be activated by the weak intrinsic bioelectric field of the prey. The high-frequency, or active,

KARGER

Fax + 41 61 306 12 34
E-Mail karger@karger.ch
www.karger.com

Accessible online at:
www.karger.com/journals/bbe

Mark E. Nelson
Beckman Institute, University of Illinois
405 N. Mathews
Urbana, IL 61801 (USA)
Tel. +1 217 244 1371, Fax +1 217 244 5180, E-Mail m-nelson@uiuc.edu

electrosense (tuberous system) is sensitive to perturbations in the fish's self-generated electric field arising from differences in impedance between the prey and the surrounding water. The extent to which each of these modalities might contribute to prey capture behavior and how information might be integrated across modalities is not well understood [reviewed in Bodznick, 1989; Coombs et al., 2002].

In weakly electric fish, active electrolocation is generally assumed to play a key role in prey detection. This assumption is based on observations that the fish detect and localize prey in the absence of visual cues, and on the predominance of peripheral and central processing devoted to the high-frequency electrosense. In an adult *A. albifrons*, for example, there are ≈14,000 high-frequency tuberous electroreceptor organs distributed over the body surface, compared with ≈700 low-frequency ampullary electroreceptor organs and ≈200 canal neuromasts (plus fewer than 30 superficial neuromasts) for the mechanosensory lateral line [Carr et al., 1982]. However, simple measures such as the total receptor count are insufficient for assessing the relative amount of behaviorally useful information conveyed by each of these different modalities. Although this paper will focus on these three modalities, we note that other non-visual, non-contact modalities might also provide useful information to the animal. Chemosensory cues could contribute to general arousal and motivation for feeding, but it is unlikely that such cues could provide the information necessary for guiding fast accurate strikes at individual planktonic prey [MacIver et al., 2001]. In principle, acoustic cues might also contribute. The potential role of the auditory system in prey detection will not be covered here [see the accompanying review by Braun et al., 2002 for more details].

Some limited experimental evidence is available regarding multimodal contributions to prey capture behavior in weakly electric fish. For *A. albifrons*, MacIver et al. [2001] found that prey detection distance varied with water conductivity over the ecologically relevant range, demonstrating that electrosensory contributions are important in mediating prey detection. They reported that the mean detection distance decreased from 28 to 13 mm with increasing conductivity in the range of 35 to 300 μS cm^{-1}, but did not change significantly above this range. This observation suggests that some other sensory modality, such as the lateral line system, might become dominant at high water conductivity, where the electric sense becomes less effective [MacIver et al., 2001]. Studies of prey search behavior in an African pulse-type weakly electric fish, *Gnathonemus petersii*, have shown that these fish can make use of information from several modalities during foraging and can use different combinations of modalities if one modality is eliminated [von der Emde and Bleckmann, 1998]. Although the precise contribution of the mechanosensory lateral line to prey detection by weakly electric fish has yet to be determined, it plays a major role in non-electroreceptive fish, especially when vision is limited [reviewed in Coombs and Montgomery, 1999; New, 2002]. Moreover, in the nocturnally active Lake Michigan mottled sculpin, the initial orienting component of prey capture behavior relies on a particular subset of lateral line organs, canal neuromasts, rather than superficial neuromasts [Coombs et al., 2001].

Analyzing electrosensory and mechanosensory contributions to prey capture behavior of weakly electric fish provides an interesting opportunity to explore multimodal interactions in closely related sensory systems. These octavolateralis systems exhibit many common features in their structural and functional organization, both at the sensory periphery as well as in central processing pathways [reviewed in Bodznick, 1989; Montgomery et al., 1995]. The prevailing view is that these similarities are largely due to common phylogenetic and ontogenetic histories [McCormick and Braford, 1988]. These systems also appear to play similar roles in many behavioral tasks, including the detection and localization of prey. Despite these similarities, it is clear that each system is dedicated to the processing of different physical stimuli with unique spatial and temporal properties. By comparing and contrasting how sensory signals are processed and integrated across these closely related systems, one can hope to gain insights into how the unique physical attributes of different stimulus modalities influence the structural, functional, and computational organization of the nervous system.

Clearly, there is much more to be learned about multimodal contributions to prey capture from carefully designed neurophysiological and behavioral studies. However, the fact that the neural and behavioral substrates of prey detection appear to be flexible and adaptive will make designing and interpreting such studies a challenging task. Our goal in this paper is to take a different approach and ask what can be learned about multimodal contributions by analyzing the problem from a modeling perspective. In particular, this paper focuses on issues associated with modeling the physical stimuli generated by the prey. At sufficiently large distances, the hydrodynamic fields as well as the electric fields associated with the prey are predominantly dipolar in nature [Kalmijn, 1997]. Higher-order multipole contributions to the field

become important only at very short distances. For *Daphnia magna*, with a diameter of 2–3 mm, dipole contributions are expected to dominate at distances larger than a few body diameters. Black ghost knifefish are typically able to detect *Daphnia* at distances of 10–30 mm [MacIver et al., 2001], hence the physical stimuli associated with the *Daphnia* can be approximated as dipolar in this range. This allows all modalities considered here to be modeled using a similar mathematical framework.

The work described here represents a subset of a more extensive modeling effort that includes sensory transduction and encoding characteristics of the peripheral receptors and afferent nerve fibers [Nelson et al., 1997; Nelson and MacIver, 1999; MacIver, 2001; Brandman and Nelson, 2002] as well as subsequent processing in the central nervous system. Although modeling studies are sometimes limited by untested assumptions and unconstrained parameters, they can nevertheless produce useful insights and provide guidance for the design of future experiments. Ultimately, experimental and modeling approaches used in close conjunction may allow us to better understand how information from multiple modalities is integrated in the central nervous system to guide complex behaviors.

Materials and Methods

The research procedures reported herein involving the use of live vertebrate animals were reviewed and approved by the Institutional Animal Care and Use Committee of the University of Illinois at Urbana-Champaign.

Behavioral Trajectories

In a previous behavioral study [MacIver et al., 2001], adult weakly electric fish of the species *Apteronotus albifrons* (12–15 cm in length) were videotaped under infrared illumination while hunting for individual aquatic prey (*Daphnia magna*, 2–3 mm in length) in the dark. A two-camera video setup provided simultaneous top- and side-views of a behavioral arena (40 × 30 × 20 cm). Selected video segments were digitized at a sampling rate of 60 frames/s. A model-based tracking system was used to accurately (± 1 mm) determine the 3D position and conformation of the fish body surface and the 3D location of the prey for each frame in the sequence [MacIver and Nelson, 2000]. Behavioral trials were carried out at four different water conductivities (35, 100, 300 and 600 μS cm^{-1}).

High-Resolution Fish Surface Model and Receptor Distribution Models

A high-resolution surface model was used for describing the surface geometry and receptor organ distribution of the fish. The polygonal surface model consists of approximately 30,000 facets with a mean facet area 0.2 mm^2 [MacIver, 2001].

The distribution of mechanosensory lateral line canal neuromasts in the model was based on empirical measurements of lateral line pore locations collected from an individual *A. albifrons* (12.7 cm in standard length). The X, Y and Z coordinates (relative to the tip of the snout) were determined for each pore using an ocular micrometer on a stereomicroscope. A total of 208 pores were identified (including both left and right sides of the fish). Of these, 12 were associated with the supraorbital canals, 14 with the infraorbital canals, 20 with the preopercular-mandibular canals, and 162 with trunk canals. The mean pore spacing was approximately 2 mm on the head and 1.3 mm on the trunk. For graphical display purposes, canal neuromasts were assumed to be located midway between adjacent pores.

The distributions of ampullary and tuberous electroreceptor organs on the model surface were based on empirical measurements reported by Carr et al. [1982] for *A. albifrons*. Diagrams and descriptions provided in this paper were used to estimate the discrete locations of 720 ampullary electroreceptor organs. For tuberous receptor organs, receptor density measurements reported from eighteen locations on the body surface were interpolated to estimate the receptor density over the entire surface. Receptor organs were randomly placed on the model surface according to the interpolated density profile. The procedure resulted in the placement of a total of 13,953 tuberous receptor organs, in good agreement with the total count estimated by Carr et al. [1982].

Modeling Mechanosensory Lateral Line Signals

Hydrodynamic images were reconstructed using previously developed simulation code [Coombs et al., 1996, 2000] originally designed to study lateral line excitation patterns in the prey capture behavior of Lake Michigan mottled sculpin [Coombs and Conley, 1997a, b; Conley and Coombs, 1998]. The prey is modeled as a dipole source (sinusoidally vibrating sphere). Hydrodynamic images are computed for each frame in the prey capture sequence. For each frame, the model produces a snapshot of the stimulation pattern when the source is at its peak acceleration. The fluid medium is assumed to be unbounded (no correction for tank walls). The source radius a and distance to the source r are both assumed to be much smaller than the wavelength $(\lambda = c/f)$. In the case of the *Daphnia* model used here, c = 1,500 m/s and f = 3 Hz, giving a wavelength of 500 m, so these constraints are well satisfied. The peak pressure at each canal pore is given by:

$$p(r,\theta) = -\frac{\rho a^3 \omega U \cos\theta}{2r^2} \quad (1)$$

where r is the distance from the dipole to the pore, θ is the angle from the dipole axis, ρ is the density of fresh water (1,000 kg/m^3), ω is the angular frequency of the source ($\omega = 2\pi f$), a is the source radius, and U is the peak source velocity. The fluid acceleration within the canal between two pores is proportional to the pressure difference between the pores according to Euler's equation:

$$a_{canal} \propto -\frac{\Delta p}{\rho \Delta l} \quad (2)$$

where Δp is the pressure difference, Δl is the pore separation and ρ is the density of fresh water. This proportionality does not take into account effects of canal diameter or canal fluid density; it is assumed that these effects are constant for all canals. The stimulus for each neuromast is taken to be proportional to the pressure difference between surrounding canal pores. The stimulus level for each neuromast was computed for each frame in the selected prey capture sequences. The neuromast stimulus level is plotted in units of accel-

eration (m/s^2) at a position along the fish's body surface that was midway between two adjacent canal pores. The effects of fish body motion, including swimming movements of the fish and possible body motion induced by prey vibration were not included in this model.

Selecting Parameters for the Mechanosensory Dipole Model

The water flows produced by *Daphnia* have been quantified by Kirk [1985] using hot-wire anemometry. Free-swimming *Daphnia* move with a jerky motion powered by sweeping movements of the antennae. The swim cycle consists of a fast downward power stroke of the antennae followed by a slower recovery phase. *Daphnia* normally swim with a slight forward pitch, such that the power stroke causes *Daphnia* to move forward and upward in the water column. During the slower recovery phase, the *Daphnia* sinks in the water column as the antennae return to their original position. The normal swimming rate is approximately 1–3 antennal beats/s, but this can increase up to 23 beats/s during escape bursts [Kirk, 1985]. Peak displacement during each stroke is on the order of the *Daphnia* radius (typically 1–2 mm). The fast jerky swimming movements of these animals gives rise to their common name of 'water flea.'

For computing hydrodynamic images, the *Daphnia* is modeled as a sinusoidally oscillating sphere. Because the actual *Daphnia* movements are asymmetric, with a fast power phase and a slow recovery phase, there are some complications to this approach. For a sinusoidal oscillation with angular frequency ω and peak displacement d, the peak velocity U is equal to ωd and the peak acceleration is ωU. If we set the oscillation frequency f = 3 beats/s, corresponding to the upper range of normal non-escape swimming [Kirk, 1985], and assume a *Daphnia* displacement of 0.002 m (corresponding to the maximum body displacement per stroke), we would compute a peak velocity of 0.04 m/s and a peak acceleration of 0.7 m/s^2. However, because the power stroke is much more rapid than the recovery stroke, the actual peak velocities and accelerations generated by *Daphnia* are much higher. Kirk [1985] reported flow velocities that are typically in the range of 0.01 m/s near the *Daphnia* with a maximum reported velocity of 0.182 m/s; the maximum reported acceleration during the rising edge of a velocity pulse was 45.85 m/s^2. Thus the estimate for acceleration ωU varies from a low of 0.7 m/s^2 based on the estimated *Daphnia* displacement and frequency to a high of approximately 46 m/s^2 based on the maximum observed value in an empirical data set. Our approach for handling this broad range of estimated values will be to model the best-case scenario by selecting parameters that result in the strongest stimulus. This same best-case strategy will also be applied to other sensory modalities.

Note that for sinusoidal motion, the source acceleration is given by ωU. To model the best-case scenario, we adjust the parameters of our model such that ωU = 46 m/s^2. Keeping the oscillation frequency fixed at f = 3 beats/s and solving for the velocity U we find U = 2.4 m/s. For simplicity, the vibrational axis of the *Daphnia* was usually taken to be vertical in world coordinates, although *Daphnia* actually tend to swim with a forward pitch. The prey radius was taken to be a = 0.0015 m.

Modeling Low-Frequency Bioelectric Fields

Planktonic prey produce weak low-frequency bioelectric fields that can activate the ampullary electrosensory system of weakly electric fish. The intrinsic bioelectric fields produced by *Daphnia* have recently been characterized for the purpose of understanding prey-related signals detected by the passive electric sense of paddlefish [Wilkens et al., 1997, 2001; Wojtenek et al., 2001a, b]. The dominant bioelectric potential generated by the *Daphnia* can be modeled as a DC dipole source with the dipole axis oriented along the posterior-anterior axis of the *Daphnia*. Mathematically, we express the electrical potential generated by the *Daphnia* as:

$$\varphi(r,\theta) = \frac{D_{prey}\cos\theta}{r^2} \quad (3)$$

where r is the distance from the dipole, θ is the angle with respect to the dipole axis, and D_{prey} is the magnitude of the *Daphnia* dipole moment. Ampullary electroreceptors respond to the voltage drop across the skin, which can be approximated by $\Delta\varphi_{skin} = \varphi(r,\theta) + c$ where c is a constant value such that the net current is zero when integrated over the entire body surface.

Selecting Parameters for Low-Frequency Bioelectric Dipole Model

Wojtenek et al. [2001a] characterized the bioelectric field of individual *Daphnia* by sweeping them past a recording electrode at a known distance, velocity and orientation. They found that the DC component of the *Daphnia* electric field could be well described by a dipole. DC potentials of up to 1 mV could be recorded near the *Daphnia*. The axis of the DC dipole was found to be oriented along the posterior-anterior axis of the *Daphnia*. In addition to the DC potential, low frequency (3–15 Hz) AC potentials were also recorded with magnitudes up to 20% of the DC potential. Some of these AC fluctuations were correlated with movements of the antennae [Wilkens et al., 1997; Wojtenek et al., 2001b].

For assessing possible contributions to prey capture behavior in weakly electric fish, we modeled the intrinsic bioelectric field of *Daphnia* as a DC dipole using equation 3. The DC potential is larger than AC potentials and is likely to dominate the detection performance of the fish; hence the AC contributions were not included in the model. It is important to realize, however, that the DC potential of *Daphnia* is transformed into an AC potential in the reference frame of the electroreceptor due to the relative motion between fish and prey [Peters et al., 1999]. For estimating the best-case dipole strength, we adjusted D_{prey} to yield a peak potential of 1 mV at a distance corresponding to the body radius (1 mm), yielding D_{prey} = 10^{-9} V·m^2. The *Daphnia* was modeled as a constant current source. According to Ohm's law, a higher resistivity will give rise to a larger voltage if the current remains constant. The empirical measurements of *Daphnia* dipole strength described above were made at a water resistivity of 2 kΩ·cm [Wojtenek et al., 2001a]. In the model, the value of D_{prey} was scaled in proportion to the water resistivity used for the behavioral trial under consideration.

The dipole axis of the bioelectric field is aligned with the body axis of the *Daphnia*. Thus, dipole orientation for the intrinsic bioelectric field was modeled in exactly the same manner as the vibrational dipole axis associated with swimming movements. For most simulations, the bioelectric dipole axis of the *Daphnia* was taken to be vertical in world coordinates because of the upright swimming posture of *Daphnia*. The voltage drop across the skin due to the *Daphnia*,, $\Delta\varphi_{skin} = \varphi(r,\theta) + c$, is computed for each receptor at each frame in the prey capture sequence. For each frame, the value of c must be recomputed to ensure that the total transdermal current is zero.

Modeling High-Frequency Electrosensory Signals

The presence of *Daphnia* creates a perturbation in the fish's self-generated electric field. To compute this perturbation, the *Daphnia* is modeled as a small sphere in a locally uniform electric field [Rasnow and Bower, 1996]. The resulting perturbation can be modeled as an induced electrical dipole centered at the prey location. The axis of the induced dipole is aligned with the local direction of the fish's electric field $\mathbf{E}_{fish}$. Considering only the resistive components of the prey impedance, the change in potential due to the prey can be written as:

$$\varphi_{prey}(r,\theta) = \frac{a^3 |\mathbf{E}_{fish}| \cos\theta}{r^2} \left(\frac{\rho_w - \rho_{prey}}{\rho_w + 2\rho_{prey}} \right) \quad (4)$$

where r is the distance from the prey, θ is the angle relative to the induced dipole axis, a is the prey radius, $\mathbf{E}_{fish}$ is the electric field vector at the location of the prey, ρ_w is the electrical resistivity of the water and ρ_{prey} is the electrical resistivity of the prey [Rasnow and Bower, 1996]. Tuberous electroreceptors respond to changes in the voltage drop across the skin, which is called the transdermal potential $\Delta\varphi_{td}$. The change in transdermal potential can be approximated by $\Delta\varphi_{td}(r,\theta) = \varphi_{prey}(r,\theta) + c$ where c is a constant such that the net transdermal current is zero when integrated over the entire body surface. The change in transdermal potential $\Delta\varphi_{td}(r,\theta)$ is computed for each receptor at each frame in the prey capture sequence. For each frame, the value of c must be recomputed to ensure that the total transdermal current is zero.

Measuring the Electrical Impedance of Daphnia magna

The term in parentheses on the right-hand side of equation 4 corresponds to the electrical contrast of the prey C_{prey}:

$$C_{prey} = \left(\frac{\rho_w - \rho_{prey}}{\rho_w + 2\rho_{prey}} \right) \quad (5)$$

If the resistivity of the prey ρ_{prey} matches the resistivity of the surrounding water ρ_w, then the electrical contrast is zero and the prey become electrically invisible. However, it should be noted that this approximation ignores possible phase shifts due to capacitive components of the prey impedance. It is also useful to consider two other limiting cases for the electrical contrast. If the prey has very low resistivity and can be approximated as an ideal conductor ($\rho_{prey} \approx 0$), then the electrical contrast $C_{prey} \approx 1$. If the prey has very high resistivity and can be approximated as an ideal insulator ($\rho_{prey} \to \infty$), then the contrast $C_{prey} \approx -\frac{1}{2}$. Thus we see that the electrical contrast changes signs depending on whether the prey is more or less resistive than the surrounding water.

To estimate the electrical contrast of the prey, empirical measurements of *Daphnia* impedance were made by placing an individual *Daphnia* in a small fluid-filled test chamber and applying sinusoidal voltages across the chamber. The test chamber was constructed of glass tubing (2 mm ID) embedded in a Plexiglas block. Brass cylindrical electrodes (2 mm OD) were gold plated, then plated with platinum black [MacIver, 2001]. The electrodes were connected to a precision LCR Meter (HP 4245A, Agilent Technologies Inc., Palo Alto, Calif., USA) that provided measurements of the magnitude and phase of the electrical impedance. Impedance was measured over a range of frequencies (0.03, 0.10, 0.3, 1, 3, 10, 30, 10, and 30 kHz) and water conductivities (100, 300, and 1000 $\mu S\ cm^{-1}$). Impedance measurements taken with the *Daphnia* suspended in water were compared with control measurements taken with water alone.

Selecting Parameters for High-Frequency Perturbations to the Self-Generated Field

Changes in transdermal potential due to the prey are modeled by equation 4. As in the mechanosensory model, the prey radius a was set to 0.0015 m. Equation 4 requires evaluating the magnitude and direction of the fish electric field vector $\vec{E}_{fish}$ at the location of the prey. Estimates of these parameters are based on empirical measurements of the electric field around an individual *A. albifrons* (9.8 cm in length) by other investigators [C. Assad, B. Rasnow, P. Stoddard, unpublished data] using the methodology described in Rasnow and Bower [1996]. The field measurements were made on dorsal and median planes extending ≈6 cm around the surface of the fish, a range that encompasses the prey strike trajectories used here [MacIver et al., 2001]. To account for changes in field strength with conductivity, the electric organ was modeled as a constant current source and the estimated field strength at the prey was scaled by the water resistivity. Over the range considered here, this approximation is in good agreement with measured changes in field strength with water conductivity for this species [Knudsen, 1975].

Results

Empirical Measurements of Daphnia Impedance

To estimate the electrical contrast of the prey C_{prey} (equation 5), we measured the impedance of individual live *Daphnia magna* in a small test cell. Figure 1 shows the electrical impedance of the test cell as a function of test frequency and water conductivity. For each test condition, the impedance was measured with and without *Daphnia.* The dashed lines show the test cell impedance for water alone and the solid lines show the impedance after introduction of a single *Daphnia*. With water alone the magnitude of the impedance $|Z|$ is fairly constant across all frequencies; once a *Daphnia* is introduced, the impedance varies in a frequency-dependent manner.

We are most interested in the *Daphnia* impedance characteristics in the frequency range of the fish's electric organ discharge, which varies from about 600–1,200 Hz, as indicated by the shaded bands in figure 1. Within this frequency band we see that adding a *Daphnia* to the test cell causes a decrease in $|Z|$ when the water resistivity is 10 k$\Omega\cdot$cm, but causes an increase in $|Z|$ when the water resistivity is 1 k$\Omega\cdot$cm. Therefore the effective resistivity of the *Daphnia* must fall between 1 and 10 k$\Omega\cdot$cm. If a *Daphnia* is added to water of 3.3 k$\Omega\cdot$cm there is almost no change in $|Z|$ within the EOD frequency band. This is the water conductivity for which the *Daphnia* become electrically invisible. Hence we set ρ_{prey} = 3.3 k$\Omega\cdot$cm when evaluating the prey contrast C_{prey} in equation 5. For example, when the water resistivity is 30 k$\Omega\cdot$cm (the highest value used in our studies), the *Daphnia* acts as a net conductor with an electrical contrast C_{prey} = 0.73.

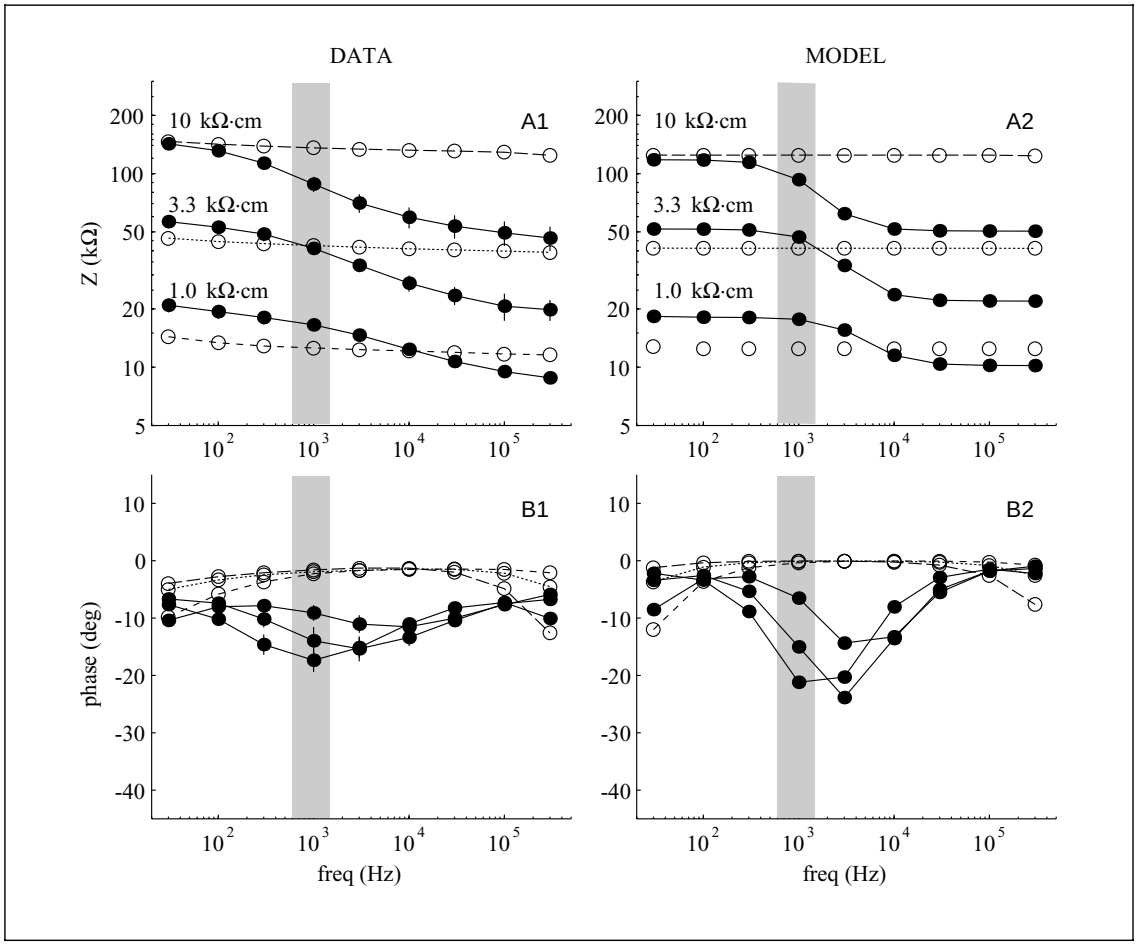

Fig. 1. Measured and modeled impedance data for live *Daphnia* at three water conductivities and nine test frequencies. These conductivities bracket the natural range found in the fish's habitat. Open symbols joined by dashed lines indicate test cell impedance with water only (no *Daphnia*); filled symbols joined by solid lines indicate impedance with live *Daphnia* in the test chamber. The shaded bands show the approximate range of electric organ discharge frequencies for *Apteronotus albifrons*. A1, B1 Experimentally measured magnitude and phase of test cell impedance. A2, B2 Magnitude and phase for the matched electrical-equivalent model.

When the water resistivity matches the prey resistivity there is no change in the magnitude of the impedance $|Z|$, but there is a detectable phase shift φ, as shown in figure 1B1. Within the EOD frequency range adding a *Daphnia* to water of 3.3 kΩ·cm causes a phase shift of about 12 degrees in the impedance of the test cell. Even when the electrical contrast goes to zero there might still be phase shifts in the electric field that could be detected by the fish [von der Emde, 1998]. However, in *Apteronotus albifrons* there are relatively few primary afferent fibers that carry this type of phase information (T-type) compared to those that carry amplitude information (P-type) [Hagiwara et al., 1965; Szabo, 1974], so only the resistive components of electrical impedance are included in the present model.

To better understand the electrical impedance characteristics of the *Daphnia*, we developed an electrical equivalent circuit model for the *Daphnia* and test cell, as shown in figure 2. The equivalent circuit for the test cell includes the capacitance of two measuring electrodes C_E, resistance of current paths through the water that are in series with the *Daphnia* R_{ws}, and resistance of current paths through the water that are in parallel with the *Daphnia* R_{wp}. The *Daphnia* is modeled as having an internal resistance R_i surrounded by a 'skin' (the carapace) with resis-

tive R_s and capacitive C_s components. The parallel and series resistances R_{wp} and R_{ws} are influenced by water resistivity as well as the extent to which the *Daphnia* fills the available volume of the test chamber. For this purpose, we considered the *Daphnia* to be a cylinder and define the diameter fraction f_d to be the ratio of *Daphnia* diameter to test chamber diameter, and the length fraction f_l to be the ratio of *Daphnia* length to test chamber length. The parameter values were adjusted using a constrained optimization algorithm to minimize the mean squared error between the real and simulated data [MacIver, 2001]. Best-fit parameter values were f_d = 0.60, f_l = 0.85, R_i = 16 kΩ, R_s = 230 kΩ, C_s = 1.2 nF. The impedance data from the matched electrical equivalent circuit model are shown in figure 1A2, B2.

Although the numerical values of the parameters are specific to this particular test cell geometry, there are some qualitative insights that can be gained from the electrical equivalent circuit model. When probed at low frequencies, the high external skin resistance of the *Daphnia* makes it appear as a net insulator relative to the surrounding water. Thus at low frequencies adding the *Daphnia* to the test cell tends to increase the overall impedance $|Z|$. When probed at sufficiently high frequencies, the high external skin resistance R_s is shunted by the low capacitive reactance of the skin $X_s = 1/(2\pi f C_s)$, and the skin essentially 'disappears' in an electrical sense. Under these conditions, the *Daphnia* appears to be a net conductor relative to the surrounding water, because the internal body fluids are more conductive than the surrounding freshwater environment. Thus at high frequencies adding the *Daphnia* to the test cell tends to decrease the overall impedance $|Z|$. At intermediate test frequencies, such as those in the EOD range of the fish, the *Daphnia* can be either a net conductor or a net insulator, depending on the resistivity of the surrounding water.

Sample Sensory Reconstructions

To this point we have established a mathematical modeling framework for describing the physical stimuli generated by the prey (equations 1–4), and we have constrained the parameters using empirical data, both from our own studies as well as those of other investigators. We now illustrate how these mathematical models of the prey source characteristics can be combined with empirically measured prey capture trajectories [MacIver et al., 2001] to reconstruct the spatiotemporal patterns of mechanosensory and electrosensory stimulation during prey capture behavior.

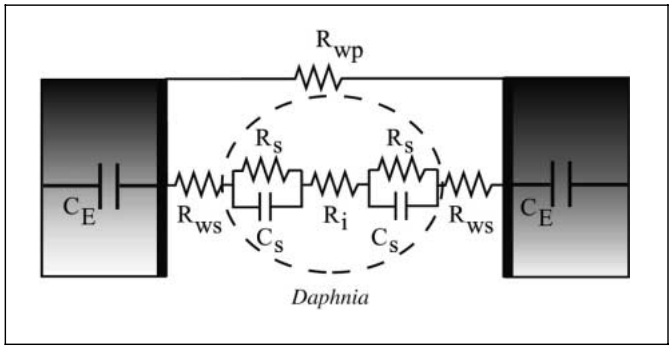

Fig. 2. An electrical equivalent model of *Daphnia* and test cell. Abbreviations: C_E, electrode capacitance; R_{wp} resistance of parallel water path; R_{ws}, resistance of series water path; R_s *Daphnia* skin (carapace) resistance; C_s *Daphnia* skin (carapace) capacitance; R_i *Daphnia* internal resistance. See text for explanation.

Figure 3 shows the spatial patterns of electrosensory and mechanosensory stimulation at four time points during a representative prey capture sequence from a trial recorded in low-conductivity water (35 μS cm^{-1}). The active electrosensory images shown in figure 3A (left column) represent the patterns of stimulation experienced by the population of tuberous electroreceptor organs. The stimulus level is expressed in terms of the change in amplitude of the local oscillatory transdermal potential established by the fish's own electric organ discharge. The passive electrosensory images shown in figure 3B (center column) represent the patterns of stimulation for ampullary electroreceptor organs, expressed as a local change in potential induced by the intrinsic bioelectric field of the prey. The mechanosensory lateral line images shown in figure 3C (right column) represent the instantaneous flow acceleration between adjacent pores in the direction of the canal at the peak of vibrational movement of the prey. Time runs vertically from top to bottom in the figure. This first row of images (t = 0 ms) represents the electrosensory and mechanosensory stimulus levels at the putative time of prey detection [MacIver et al., 2001]. At this time, the prey is located approximately 2.7 centimeters above the dorsum of the fish. The fish is swimming forward with a longitudinal velocity of 15.9 cm/s. The fish is oriented with the head pitched downward and the tail bent to the left. In the next row (t = 200 ms after detection) the fish has reversed swimming direction and is now swimming backwards with a longitudinal velocity of –3.7 cm/s. The prey is about 1.4 cm from the receptor surface and stimulus levels in all three modalities are well

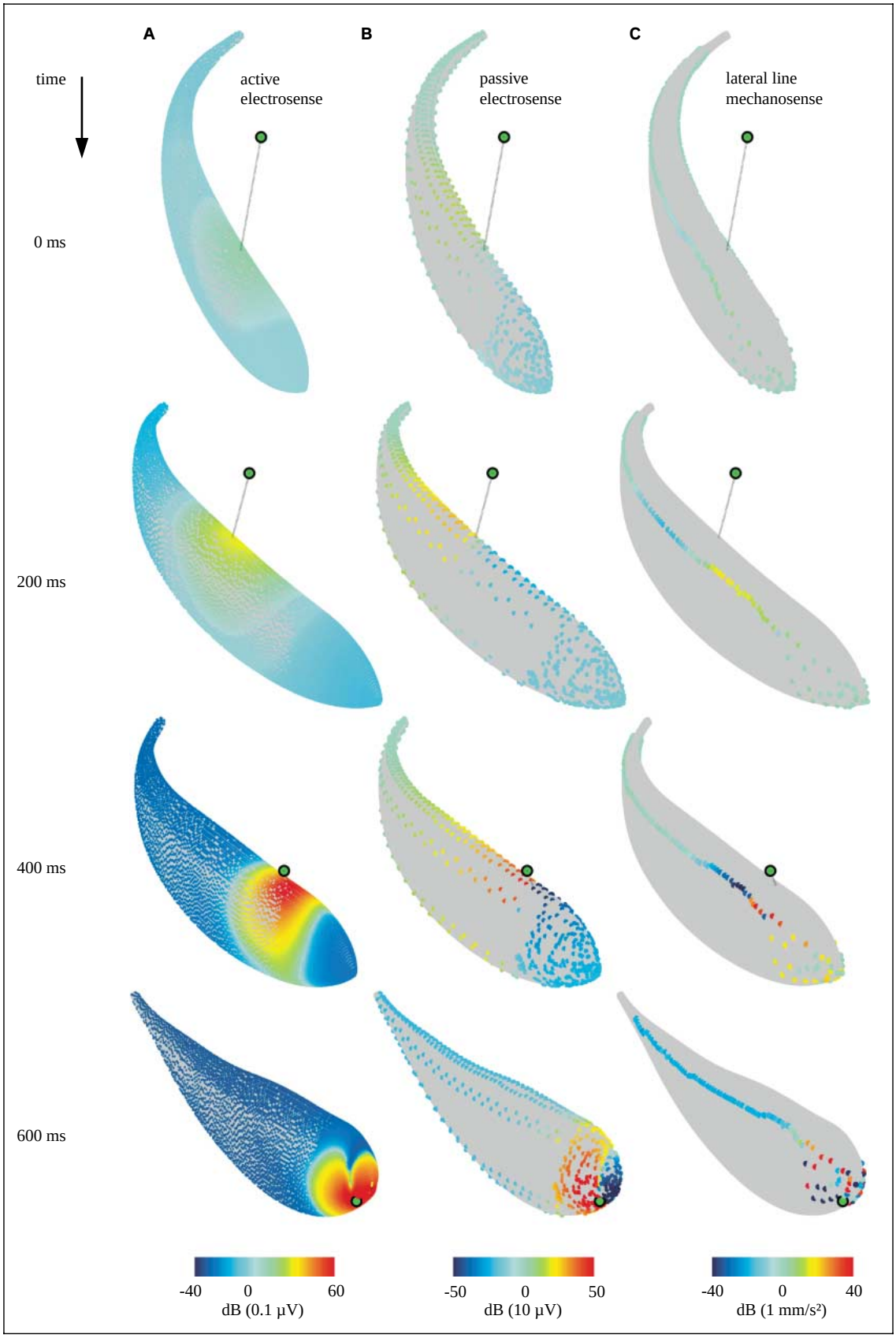
A
B
C
time
active
electrosense
passive
electrosense
lateral line
mechanosense
0 ms
200 ms
400 ms
600 ms
-40
0
60
dB (0.1 µV)
-50
0
50
dB (10 µV)
-40
0
40
dB (1 mm/s²)

above the estimated threshold levels. In the third row (t = 400 ms after detection), the fish is moving backwards rapidly at a velocity of –11.3 cm/s and the mouth of the fish is approaching the prey. At this point the prey is about 0.4 cm from the receptor array; and the electrosensory and mechanosensory images are much stronger and more focal. In the bottom row (t = 600 ms after detection) the fish is about to make a final lunge and engulf the prey. At this point the prey is only a few millimeters from the mouth. The images are very intense and confined largely to the head region of the fish.

Discussion

Reconstructing the dynamic spatiotemporal patterns of stimulation across multiple sensory modalities holds great promise for expanding our understanding of how these different modalities contribute to prey capture behavior and what sorts of information processing demands are placed on the system. At this stage of development of the models it is premature to make detailed quantitative comparisons among the different modalities. The current framework still contains a number of untested assumptions and weakly constrained parameters. For example, for all three modalities we assumed that the electrical and mechanical properties of the fish's body could be ignored when computing the stimulus patterns generated by the prey. There is some empirical evidence that such modeling approximations are reasonable for the tuberous electrosensory system [Rasnow and Bower, 1996] and for the lateral line canal system when the fish is stationary [Coombs et al., 1996]. For a moving fish, however, effects of the fish's self-generated swimming motions need to be taken into account, as the actual stimulus to the lateral line canal system is the net acceleration between fish and surrounding water. In general, it is useful to distinguish between two kinds of errors introduced by modeling uncertainties. Many of these uncertainties will lead to errors in an estimate of the overall stimulus amplitude, but will not alter the fundamental spatiotemporal patterns of stimulation. Uncertainties in overall stimulus amplitude will influence assessment of the relative contributions of different modalities, but will not significantly alter our analysis of the spatial and temporal image characteristics.

In terms of analyzing the stimulus magnitude, it is important to realize that the image intensity falls rapidly with increasing distance for all three modalities; hence these are all short-range senses. The simplest case to analyze is the ampullary system, where the bioelectric potential generated by the *Daphnia* falls as r^{-2} (equation 3). The ampullary electroreceptors respond to the gradient of the potential, which therefore falls as r^{-3}. Comparing the stimulus intensity when the prey is 10 cm from the fish (approximately one body length), versus 1 cm from the fish (a typical detection distance), one finds that the peak stimulus intensity falls by a factor of 1000 over this range. For the tuberous electrosensory system, it initially appears from equation 4 that the change in electrical potential induced by the prey also falls as r^{-2}. However, there is an additional distance-dependent term in equation 4 arising from the fact that the perturbation is proportional to the fish's electric field strength $|\mathbf{E}_{fish}|$ at the location of the prey. Because the fish's own field strength also falls off with distance, the change in electrical potential induced by the prey is expected to fall approximately as r^{-3} rather than r^{-2} in the range of 1–10 cm from the fish, as has been measured empirically for small spherical objects placed in the fish's field [Rasnow and Bower, 1996]. The tuberous electroreceptors respond to the gradient of this potential, which therefore falls as r^{-4}. Thus we find that the stimulus intensity falls more rapidly with distance for the tuberous system ($\approx r^{-4}$) than for the ampullary system ($\approx r^{-3}$).

For the mechanosensory system, pressure generated by the swimming movements of the prey falls as r^{-2} (equation 1). The lateral line canal neuromasts respond to the local pressure gradient (Equation 2), which falls as r^{-3}. However, if one takes the fish's body motion into account (which was not included in these simulations), the effective stimulus (net acceleration between fish and surround-

Fig. 3. Selected 'snapshots' from a representative prey strike trajectory showing reconstructed active electrosensory, passive electrosensory, and mechanosensory images at four time points along the trajectory. Time (ms) runs vertically from top to bottom; times are measured relative to the putative time of prey detection (t = 0). The green filled circle indicates the location of the prey (*Daphnia magna*); the dotted line indicates the shortest line to the fish surface. A Stimulus levels for 13,953 tuberous electroreceptor organs, expressed as the change in amplitude of the local transdermal potential. B Stimulus levels for 720 ampullary electroreceptor organs, expressed as the magnitude of the bioelectric field of the prey at the fish surface. C Stimulus levels for 208 lateral line canal neuromasts, expressed as canal particle acceleration. Images are shown on a logarithmic color scale in units of decibels; the 0 dB reference is taken to be the estimated threshold sensitivity (active electrosensory: 0.1 μV, passive electrosensory: 10 μV, mechanosensory: 1 mm/s^2). Negative values indicate opposite stimulus polarity (not smaller signal magnitude).

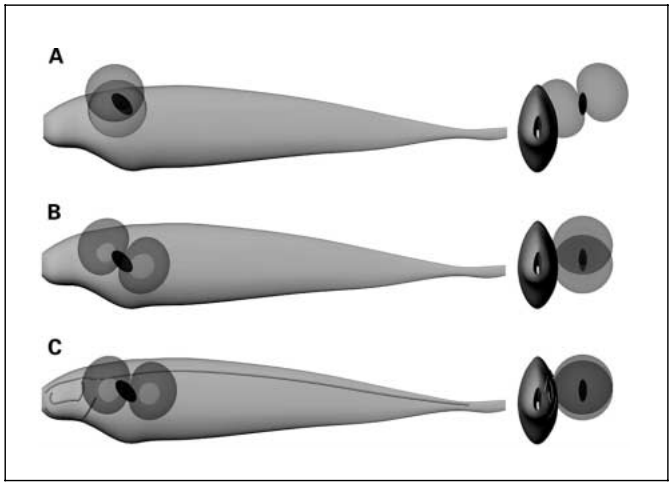

Fig. 4. Schematic illustration of differences in stimulus dipole orientation for different modalities. The left-hand column shows a lateral view of the fish; the right-hand column shows a head-on view of the fish. A Tuberous electroreceptors associated with the active electric sense are stimulated by a dipole oriented along the direction of the fish's self-generated electric field, which tends to be normal to the fish's body surface. B Ampullary electroreceptors associated with the passive electrosensory system are stimulated by the intrinsic bioelectric dipole of the prey, which is aligned with the prey body axis. C The mechanosensory lateral line system is stimulated by a vibrational dipole that is aligned with prey body axis when the fish is stationary. The canal neuromasts are stimulated by the gradient of the dipole field in the direction of the canals (indicated by gray lines), which run parallel to the body surface.

ing water) falls as r^{-4}. From the point of view of prey capture behavior, where the distance between fish and prey is steadily decreasing as the fish approaches the prey [MacIver et al., 2001], the power-law scaling behavior for all three modalities means that the strength of the stimulus grows extremely rapidly as the fish approaches the prey.

Regarding the spatial patterns of stimulation there are a couple of noteworthy points. Because the physical stimulus for all three modalities can be approximated as a dipole field, one might expect that the spatial patterns of stimulation would be quite similar as well. However, this is not the case. As illustrated in figure 4, the orientation of the stimulus dipole relative to the receptor array has an important influence on the spatial pattern of stimulation. For tuberous electrosensory stimuli, the orientation of the stimulus dipole is determined by the direction of the fish's electric field $\mathbf{E}_{fish}$ at the prey's location, rather than by orientation of the *Daphnia* body axis. Near the head and rostral trunk region of the fish, the local electric field vectors $\mathbf{E}_{fish}$ tend to be oriented approximately normal to the receptor surface [Rasnow and Bower, 1996]. If the equipotential lines around the induced dipole are envisioned as a two-lobed, dumbbell-shaped structure, then the dumbbell is oriented such that the receptor surface typically slices through one end of a single lobe, as illustrated in figure 4A. The resulting tuberous electrosensory image is approximately a unimodal 'bump' on the sensory surface, as illustrated in figure 3A. (The tuberous image isn't strictly unimodal; it actually has a slight 'Mexican hat' shape with a strong central peak and a weak surrounding region of opposite polarity.) For ampullary electrosensory stimuli, the orientation of the dipole stimulus is dependent on the orientation of the *Daphnia* body axis [Wojtenek et al., 2001a]. In this case, the receptor surface can slice through one or both lobes of the dipole field depending on the orientation of the *Daphnia*, as illustrated in figure 4B. When the receptor surface slices through both lobes of the dipole, the resulting ampullary electrosensory images are bimodal, as illustrated in figure 3B.

Finally, for mechanosensory stimuli the stimulus can be described as a dipole oriented along the prey body axis, provided that the fish itself is stationary [Coombs et al., 1996, 2001]. In the absence of any hydrodynamic currents generated by movements of the fish, the *Daphnia* is the sole source of the dipole field. In this case, the lateral line canals can slice through one or both lobes of the dipole field depending on the relative position and orientation between the canal and the *Daphnia* body axis, as illustrated in figure 4C. This gives rise to more complex spatial patterns of the pressure gradient; the resulting stimulation patterns along the length of the canal can be unimodal, bimodal or trimodal. For swimming fish that generate their own hydrodynamic currents, the resulting pattern of mechanosense stimulation will depend on the interaction between two dipole sources – the fish and the *Daphnia.* Even though dipole orientations for both ampullary and lateral line stimuli are related to the *Daphnia* body axis, the resulting patterns of stimulation at the sensory surface can be quite different. This is because the lateral line system responds to the gradient of the dipole field along the canal direction, parallel to the body surface, whereas the ampullary receptors respond to the gradient of the dipole field across the skin, which is perpendicular to the body surface.

A final point about the spatial patterns is that sensory images are blurred for all three modalities. When the prey is far from the receptor array, the pattern of stimulation is weak and diffuse; as the prey comes closer to the sensory surface the image becomes progressively sharper and stronger. This transition from weak diffuse images to

strong focal images takes place over a time scale of less than one second during a typical prey capture event [MacIver et al., 2001]. This has potential implications for how information about prey location and distance is encoded and how the central nervous system should optimally process sensory data to extract the most useful information. If sensory data are being used solely for *detection* of the prey when images are weak and diffuse, then one would expect to find central neurons with large spatial receptive fields that pool data from large regions of the sensory array. On the other hand, if sensory data are being used for precise *localization* of the prey during the phase when images are strong and focal, then one might expect to find central neurons with small focal receptive fields. An alternative but not mutually exclusive idea is that the relative stimulation of central neurons with different-sized spatial receptive fields might encode prey distance. The stimulation of central neurons with large spatial receptive fields would signify far distances, whereas the stimulation of central neurons with small receptive fields would signify near distances. Interestingly, the tuberous electrosensory system contains multiple maps in the brainstem electrosensory nucleus with different spatial and temporal filtering properties [Heiligenberg and Dye, 1982; Shumway, 1989a, b], whereas the ampullary electrosensory system and the lateral line system each have a single brainstem map. The functional significance of this difference in organization across modalities has not yet been determined [Coombs et al., 2002], but information on the spatiotemporal image properties during prey capture behavior should prove useful in interpreting physiological studies of receptive field structure across sensory modalities.

The modeling results suggest that all three modalities can potentially contribute to prey localization and capture and that the relative contributions might change as a function of environmental conditions (e.g., water conductivity) and as a function of time over the course of the prey capture event. Because of the unique physical attributes of the different stimulus modalities, the information provided by these systems are both overlapping and complementary. Spatial stimulation patterns in all three systems convey information related to prey location and distance. The tuberous electrosense seems particularly well suited for extracting this information because the spatial patterns tend to be less complex and independent of other confounding variables such as prey body axis orientation. In addition, the tuberous system has a much higher density of peripheral receptors and more complexity in central nervous system processing associated with multiple maps in the brainstem. The tuberous electrosense also provides information on prey impedance, which might help the fish discriminate between different prey and non-prey objects in the environment. In addition to prey location and distance, the ampullary electrosense could also provide information on prey orientation due to the fact that the dipole axis of the bioelectric field is aligned with the prey body axis. Furthermore, the AC and DC characteristics of the bioelectric field might provide useful cues for object discrimination. The lateral line canal system also conveys cues related to location, distance and prey orientation, as well as providing instantaneous information on the relative direction (and possibly acceleration) of prey movement. All of this multimodal information is provided to the central nervous system by parallel input pathways. The spatiotemporal coherence of the signals and complementarity of features encoded by these multiple modalities should allow them to act together in a synergistic way to enhance overall detection, localization and discrimination performance. Exploring the behavioral, physiological and anatomical substrates for such multimodal interactions remains a fruitful area for future experimental and modeling studies.

Acknowledgments

This work was supported by NSF grant IBN-0078206 and NIH grant R01-MH49242 to M.E.N. We would also like to thank Ms. Alexi Metz for her contributions to mapping the pore distributions for the lateral line canal system.

References

Bodznick, D. (1989) Comparisons between electrosensory and mechanosensory lateral line systems. *In* The Mechanosensory Lateral Line: Neurobiology and Evolution (ed. by S. Coombs, P. Görner and H. Münz), Springer, New York, pp. 653–678.

Brandman, R., and M.E. Nelson (2002) A simple model of long-term spike train regularization. Neural Comp., *14:*1575–1597.

Braun, C.R., S. Coombs, and R.R. Fay (2002) What is the nature of multisensory interaction between octavolateralis sub-systems? Brain Behav. Evol., *59:* 162–176.

Carr, C.E., L. Maler, and E. Sas (1982) Peripheral organization and central projections of the electrosensory nerves in gymnotiform fish. J. Comp. Neurol., *211:* 139–153.

Conley, R.A., and S. Coombs (1998) Dipole source localization by mottled sculpin. III. Orientation after site-specific, unilateral denervation of the lateral line system. J. Comp. Physiol. A, *183:* 335–344.

Coombs, S., and R.A. Conley (1997a) Dipole source localization by mottled sculpin. I. Approach strategies. J. Comp. Physiol. A, *180:* 387–399.

Coombs, S., and R.A. Conley (1997b) Dipole source localization by mottled sculpin. II. The role of lateral line excitation patterns. J. Comp. Physiol. A, *180:* 401–415.

Coombs, S., and J.C. Montgomery (1999) The enigmatic lateral line system. *In* Comparative Hearing: Fishes and Amphibians (ed. by A.N. Popper and R.R. Fay) Springer Handbook of Auditory Research, Vol. 11, Springer, Berlin, pp. 319–362.

Coombs, S., M. Hastings, and J. Finneran (1996) Modeling and measuring lateral line excitation patterns to changing dipole source locations. J. Comp. Physiol. A, *178:* 359–371.

Coombs, S., J.J. Finneran, and R.A. Conley (2000) Hydrodynamic imaging by the lateral line system of the Lake Michigan mottled sculpin. Phil. Trans. R. Soc. Lond., *355:* 1111–1114.

Coombs, S., C.B. Braun, and B. Donovan (2001) Orienting response of Lake Michigan mottled sculpin is mediated by canal neuromasts. J. Exp. Biol., *204:* 337–348.

Coombs, S., J. New, and M.E. Nelson (2002) Information-processing demands in electrosensory and mechanosensory lateral line systems. J. Physiol.-Paris., in press.

Hagedorn, M. (1986) The ecology, courtship and mating of gymnotiform electric fish. *In* Electroreception (ed. by T.H. Bullock and W. Heiligenberg), Wiley, New York, pp. 497–525.

Hagiwara, S., T. Szabo, and P.S. Enger (1965) Electroreceptor mechanisms in a high-frequency weakly electric fish, *Sternarchus albifrons*. J. Neurophysiol., *28:* 784–799.

Heiligenberg, W., and J. Dye (1982) Labelling of electroreceptive afferents in a gymnotoid fish by intracellular injection of HRP: The mystery of multiple maps. J. Comp. Physiol., *148:* 287–296.

Kalmijn, A.J. (1997) Electric and near-field acoustic detection, a comparative study. Acta Physiol. Scand. *161*, Suppl. *638:* 25–38.

Kirk, K.L. (1985) Water flows produced by *Daphnia* and *Diaptomus*: Implications for prey selection by mechanosensory predators. Limnol. Oceanogr., *30:* 679–686.

Knudsen, E. (1975) Spatial aspects of the electric fields generated by weakly electric fish. J. Comp. Physiol., *99:* 103–118.

MacIver, M.A. (2001) The computational neuroethology of weakly electric fish: body modeling, motion analysis, and sensory signal estimation. Ph.D. dissertation, University of Illinois, Urbana-Champaign, IL.

MacIver, M.A., and M.E. Nelson (2000) Body modeling and model-based tracking for neuroethology. J. Neurosci. Meth., *95:* 133–143.

MacIver, M.A., N.M Sharabash, and M.E. Nelson (2001) Prey-capture behavior in gymnotid electric fish: Motion analysis and effects of water conductivity. J. Exp. Biol., *204:* 543–557.

McCormick, C.A., and M.R. Braford Jr. (1988) Central connections of the octavolateralis system: evolutionary considerations. *In* Sensory Biology of Aquatic Animals (ed. by J. Atema, R.R. Fay, A.N. Popper and W.N. Tavolga), Springer, New York, pp. 341–364.

Montgomery, J.C., S. Coombs, R.A. Conley, and D. Bodznick (1995) Hindbrain sensory processing in lateral line, electrosensory and auditory systems: A comparative overview of anatomical and functional similarities. Aud. Neur., *1:* 207–231.

Nelson, M.E., and M.A. MacIver (1999) Prey capture in the weakly electric fish *Apteronotus albifrons*: Sensory acquisition strategies and electrosensory consequences. J. Exp. Biol., *202:* 1195–1203.

Nelson, M.E., Z. Xu, and J.R. Payne (1997) Characterization and modeling of P-type electrosensory afferent responses to amplitude modulations in a wave-type electric fish. J. Comp. Physiol. A, *181:* 532–544.

New, J.G. (2002) Multimodal integration in the feeding behaviors of predatory teleost fishes. Brain Behav. Evol., *59:* 177–189.

Peters, R.C., W.J.G. Loos, F. Bretschneider, and A.B. Baretta (1999) Electroreception in catfish: patterns from motion. Belg. J. Zool., *129:* 263–268.

Rasnow, B., and J.M. Bower (1996) The electric organ discharges of the gymnotiform fishes: I. *Apteronotus leptorhynchus*. J. Comp. Physiol. A, *178:* 383–396.

Shumway, C. (1989a) Multiple electrosensory maps in the medulla of weakly electric gymnotiform fish. I. Physiological differences. J. Neurosci., *9:* 4388–4399.

Shumway, C. (1989b) Multiple electrosensory maps in the medulla of weakly electric gymnotiform fish. II. Anatomical differences. J. Neurosci., *9:* 4400–4415.

Szabo, T. (1974) Anatomy of the specialized lateral line organs of electroreception. *In* Electroreceptors and Other Specialized Receptors in Lower Vertebrates (ed. by A. Fessard), Handbook of Sensory Physiology, Vol. III/3, Springer, Berlin, pp. 13–58.

von der Emde, G. (1998) Capacitance detection in the wave-type electric fish *Eigenmannia* during active electrolocation. J. Comp. Physiol. A *182:* 217–244.

von der Emde, G., and H. Bleckmann (1998) Finding food: senses involved in foraging for insect larvae in the electric fish *Gnathonemus petersii*. J. Exp. Biol., *201:* 969–980.

Wilkens, L.A., D.F. Russell, X. Pei, and C. Gurgens (1997) The paddlefish rostrum functions as an electrosensory antenna in plankton feeding. Proc. R. Soc. Lond. B, *264:* 1723–1729.

Wilkens, L.A., B. Wettring, E. Wagner, W. Wojtenek, and D.F. Russell (2001) Electrosensory detection is sufficient for selective feeding by the paddlefish. J. Exp. Biol., *204:* 1381–1389.

Winemiller, K.O., and A. Adite (1997) Convergent evolution of weakly electric fishes from floodplain habitats in Africa and South America. Environ. Biol. Fishes, *49:* 175–186.

Wojtenek, W., M.H. Hofmann, and L.A. Wilkens (2001a) Primary afferent electrosensory neurons represent paddlefish natural prey. Neurocomputing, *38:* 451–458.

Wojtenek, W., X. Pei, and L.A. Wilkens (2001b) Paddlefish strike at artificial dipoles simulating the weak electric fields of planktonic prey. J. Exp. Biol., *204:* 1391–1399.